Investigation of antimagnetic rotation in light Cadmium nuclei: ^{106,108}Cd

A. J. Simons,[1] R. Wadsworth,[1] D. G. Jenkins,[1] R. M. Clark,[2] M. Cromaz,[2] M. A. Deleplanque,[2]
R. M. Diamond,[2] P. Fallon,[2] G. J. Lane,[2,*] I. Y. Lee,[2] A. O. Macchiavelli,[2] F. S. Stephens,[2]
C. E. Svensson,[2,†] K. Vetter,[2,‡] D. Ward,[2] S. Frauendorf,[3,4] and Y. Gu[3]
[1]*Department of Physics, University of York, Heslington, York Y010 5DD, United Kingdom*
[2]*Nuclear Science Division, Lawrence Berkeley National Laboratory, Berkeley, California 94720, USA*
[3]*Department of Physics, University of Notre Dame, Notre Dame, Indiana, 46556, USA*
[4]*FZ Rossendorf, Postfach 510119, D-01314, Dresden, Germany*
(Received 14 March 2005; published 30 August 2005)

The lifetimes of excited states belonging to the lowest lying positive-parity bands in ^{106,108}Cd have been measured using the Doppler-shift attenuation method. The resulting $B(E2)$ transition rates show a significant decrease with increasing spin in ^{106}Cd, whereas in ^{108}Cd there is tentative evidence for a similar effect. The results are compared with cranking and semiclassical model calculations, which indicate that the structures have the properties expected from an "antimagnetic" rotational band resulting from the coupling of $g_{9/2}$ proton holes to aligned pairs of $h_{11/2}$ and $g_{7/2}$ neutron particles.

DOI: 10.1103/PhysRevC.72.024318 PACS number(s): 21.10.Tg, 23.20.Lv, 25.70.Gh, 27.60.+j

I. INTRODUCTION

In nuclei the existence of regular rotational bands consisting of stretched $E2$ transitions is usually interpreted as arising from the coherent collective rotation of many nucleons about an axis perpendicular to the symmetry axis [1]. Such nuclei are usually well deformed. Over the past few years a new type of rotational band, consisting of magnetic dipole ($M1$) transitions in nearly spherical nuclei, has been discovered in the light lead and cadmium/tin isotopes as well as in other groups of nuclei (see Refs. [2,3]). The intriguing feature here is that the orientation of these rotors is specified by the current distribution of the high-j nucleons involved in the configurations rather than by their overall nuclear density distribution. This has been verified through lifetime measurements, which indicate that these structures have very small quadrupole deformation (e.g., see Refs. [4,5]). For these nuclei the current loops of the valence nucleons break the isotropy, as illustrated in Fig. 1(a). These loops generate a magnetic dipole vector that rotates and produces the strong $M1$ transitions. The name "magnetic rotation" was given to this phenomenon, because it is the current loops and the magnetic dipole that are rotating in space. For these structures the angular momentum vector of the valence proton particles is perpendicular to that resulting from the valence neutron holes at the band head, a feature that has been demonstrated by measurements of the g factor of the bandhead of such a structure in ^{197}Pb [6]. The resulting proton and neutron vectors form the blades of a pair of shears and the total angular momentum increases along the band by closing the blades of these shears. The existence of this "shears mechanism" [7] has been firmly established by measuring the $B(M1)$ values of the magnetic transitions, which rapidly decrease as the shears close and the transverse component of the magnetic dipole moment decreases. These structures are therefore also known as "shears bands." More extensive discussions of such bands and their properties can be found in Refs. [2,3].

A different arrangement of the high-j proton hole and neutron particle current loops, which also breaks the axial symmetry about the total angular momentum vector, is also possible. Such an arrangement is shown in Fig. 1(b). This type of coupling leads to a new phenomenon in near-spherical nuclei. The configuration can be considered as being composed of two "magnetic" subsystems [each consisting of one protonhole and one neutron particle in the example shown in Fig. 1(b)] of the magnetic type. The transverse magnetic moments of the magnetic subsystems are anti-aligned. The resulting transverse magnetic moment is zero; that is, there is no electromagnetic $M1$ radiation, which is characteristic for magnetic rotation. To account for this, a new mode called "antimagnetic rotation" [8] was proposed. In the case of magnetic rotation, the angle of rotation about the angular momentum vector is specified by the total transverse magnetic moment or by the orientation of the two crossed current loops. In the case of antimagnetic rotation, the angle of rotation is specified by the transverse magnetic moment of one of the magnetic subsystems or by the orientation of the current loops that are perpendicular to the angular momentum axis (the two proton holes in our case).

There is a certain analogy to the orientation of the atomic spins in ferromagnetism and antiferromagnetism. In the case of a ferromagnet, all atomic magnetic moments are aligned, resulting in the macroscopic magnetic moment that specifies the orientation of the system. In the case of an antiferromagnet, one half of the atomic dipole moments are aligned on one sublattice, and the other half are aligned in the opposite direction on the second sublattice in crystalline cubic structures. Although the net magnetic moment is zero, the magnetic moment of one of the sublattices specifies the orientation of the system. However, the analogy is not complete, because the longitudinal component of the magnetic moment of an antimagnetic rotor is large.

*Present address: Department of Nuclear Physics, Australian National University, Canberra, ACT 2000, Australia.
†Present address: Department of Physics, University of Guelph, Guelph, Ontario N1G 2W1, Canada.
‡Present address: Glen T. Seaborg Institute, Lawrence Livermore National Laboratory, Livermore, California, 94550, USA.

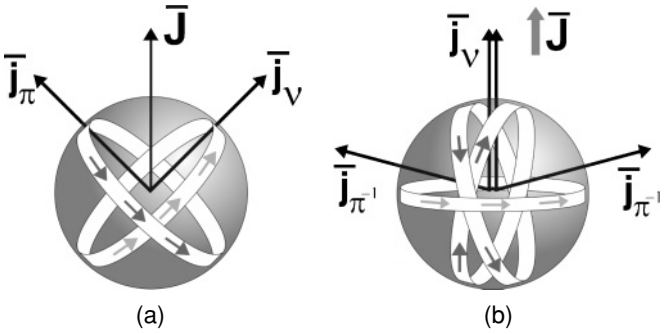

FIG. 1. Schematic figure showing the shears mechanism for (a) magnetic and (b) antimagnetic rotors. $\underline{\mathbf{J}}$ is the total intrinsic angular momentum vector and $\bar{\mathbf{j}}_\pi$ and $\bar{\mathbf{j}}_\nu$ are the proton and neutron components, respectively. Note that the two lines shown for $\bar{\mathbf{j}}_\nu$ in (b) represent the aligned neutrons and reflect the discussion given in the introduction regarding the composition of the proton and neutron vectors in an antimagnetic rotor. Both figures show the near-bandhead configuration for each type of mechanism.

In the mass-100 region the two reorienting blades of the shears in the antimagnetic rotor are formed from the angular momentum vectors of two $g_{9/2}$ proton holes [see Fig. 1(b)]. An increase in the total angular momentum is generated by the simultaneous closing of these two blades along the direction of the total angular momentum vector, which also contains the vector resulting from the aligned neutron particles involved in the configuration. Since the "antimagnetic" rotor is symmetric with respect to a rotation of π about the angular momentum axis, the bands consist of regular sequences of energy levels differing in spin by $2\hbar$. Furthermore, they should decay by weak electric quadrupole ($E2$) transitions, reflecting the weakly deformed core. Additional signatures include a rapid decrease of the $B(E2)$ values with increasing spin, which results in a rapid increase in the ratio of the dynamic moments of inertia $\mathcal{J}^{(2)}$ to the reduced transition probability $B(E2)$ values with increasing spin. A more detailed discussion of this latter feature will be presented later in this paper. The last two features can clearly be demonstrated by measuring lifetimes of states within an antimagnetic band.

Following earlier predictions [2], the first firm evidence for antimagnetic rotation has recently been reported in the yrast positive-parity band in ^{106}Cd [9], although an earlier paper on ^{100}Pd [10] reported the first tentative evidence for this phenomenon. The present paper focuses in more detail on the interpretation of the results in ^{106}Cd and also presents new lifetime measurements for the equivalent band in ^{108}Cd. (Following the submission of the present paper results on the lifetimes of excited states in the positive-parity yrast band were published [11]. These generally show good agreement with the values obtained in the present work.)

II. EXPERIMENTAL DETAILS AND DATA ANALYSIS

High-spin states in ^{106,108}Cd were populated using the ^{62}Ni(^{48}Ca,4n) and ^{96}Zr(^{16}O,4n) reactions at beam energies of 183, 207, and 72 MeV, respectively. The 183-MeV ^{48}Ca beam, accelerated by the 88-in. cyclotron at the Lawrence Berkeley National Laboratory, was incident on an enriched 979 μg/cm^2 ^{62}Ni target on a backing of 18 mg/cm^2 of gold. The resulting γ decay was detected by the Gammasphere array [12], which contained 95 hyperpure Ge detectors for this experiment. At the higher beam energy a single self-supporting ^{62}Ni foil of 520 μg/cm^2 was used. A total of $\sim 2 \times 10^8$ events of threefold or higher coincidences were collected in the backed target data set, whereas $\sim 5 \times 10^8$ such events were obtained from the thin target experiment. The Gammasphere array, containing 100 hyperpure Ge detectors was also used for the ^{108}Cd experiment. In this case the target consisted of 500 μg/cm^2 ^{96}Zr mounted onto a 10 mg/cm^2 thick natural lead backing. Approximately 5×10^8 events were recorded with a suppresssed germanium fold $\geqslant 3$. In each case the high-fold γ-ray data were unfolded into triples events and sorted into γ-gated angle-dependent γ-γ correlation matrices. The triples data were sorted into E_γ-E_γ-E_γ cubes to confirm the published decay schemes and also to obtain the side-feeding intensities of the structures of interest.

Lifetimes were extracted for levels in the positive-parity bands in ^{106,108}Cd by fitting the Doppler-broadened line shapes of γ rays using the LINESHAPE analysis code of Wells and Johnson [13]. The slowing down of the recoiling nuclei in the target and gold/lead backings was simulated using Monte Carlo methods with 5000 histories and a time step of 1 fs and treated according to the prescription of Gascon *et al.* [14]. The tables of Northcliffe and Schilling [15], with shell corrections, were used for the electronic stopping powers. The histories were used to create velocity distributions for particular angular groups of detectors at an averaged angle based on the geometry of the Gammasphere array. Calculated line shapes for each transition were obtained in the following manner: First, it was assumed that there was 100% side-feeding into the top of the band in both nuclei via a cascade of five transitions with the same moment of inertia as the in-band transitions. The highest γ ray for which a line shape was observed was then fitted and the extracted effective lifetime of the state from which this transition emerged was then used as an input parameter to extract the lifetimes of states lower in the cascade. Side-feeding into each of the lower states was also assumed using a similar rotational cascade of five transitions. In the fitting procedure the quadrupole moments of the side-feeding cascades were allowed to vary, which when combined with the moment of inertia yielded effective side-feeding lifetimes for each level under investigation.

The energies of the γ rays and the side-feeding intensities were used as input parameters for the line-shape analysis. For ^{106}Cd, side-feeding intensities were determined from the thin target data and those were compared with the values obtained in Ref. [16]. In all but one case, there was good agreement between the two sets of values. The main discrepancy was for the intensity feeding the 18^+ state, with the value from Ref. [16] being 33% whereas that from the present experiment was 15%. The latter value was used in the present work. In the case of ^{108}Cd the side-feeding intensities were determined from Ref. [17] for states up to spin 18. For the higher states the intensities were estimated from the backed target data obtained in the present work. These were found to be approximately 50%.

Line-shape fits were performed for detectors located at averaged angles of 52.8°, 90°, 127.2° and 34.6°, 90°, 145.4°.

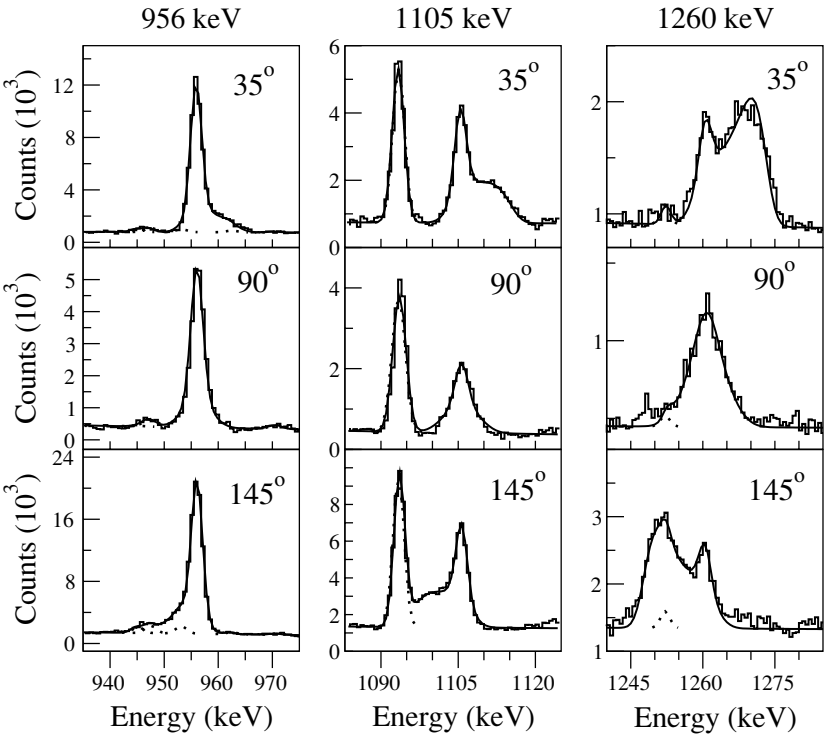

FIG. 2. Representative spectra and fitted line shapes (solid lines) for the 956-, 1105-, and 1260-keV γ rays in the yrast band of ^{108}Cd. Dashed lines show contaminant peaks. The spectra shown are taken from averaged forward 31.72° and 37.34° ($\overline{\theta} = 34.57°$) rings (top), the 90° ring (middle), and averaged backward 142.62° and 148.28° ($\overline{\theta} = 145.45°$) rings (bottom).

In each case simultaneous fits to forward, backward, and transverse spectra were made. Typical line-shape fits for the new data in ^{108}Cd are shown in Fig. 2. Examples of fits for ^{106}Cd can be found in Fig. 2 of Ref. [9]. For each line-shape combination given here the background parameters in the vicinity of the peaks, of interest, the intensities of contaminant peaks, and the in-band and side-feeding quadrupole moments were allowed to vary. The χ^2 minimization routines of MINUIT [18] were then used to fit the simulated line shapes to the experimental data. Once the minimum χ^2 was achieved the background and stopped contaminant peak parameters were fixed. The lifetimes of each state and its associated side-feeding were then deduced from a global fit of the full cascade with independently variable quadrupole moments for each state (except the topmost state) and the associated side-feeding cascades. For both nuclei the side-feeding lifetimes were found to be comparable to or up to 20% slower than the in-band lifetimes.

The uncertanties in the lifetimes were obtained from the behavior of the χ^2 value in the vicinity of the minimum using the MINOS routine [18], which finds the true errors (confidence intervals) by examining the behavior of χ^2 as each free parameter is varied independently in the location of its best value. As already indicated, the only parameters allowed to vary during the final cascade-fitting procedure were the side-feeding quadrupole moments and the quadrupole moments of the states under investigation. The final values of the lifetimes, which are presented in Table I, were obtained by taking weighted averages of the results obtained from the two separate fits that were performed. It should be noted that the errors in the table do not account for additional systematic uncertainties, which may be as large as ±20% and arise from the choice of stopping powers used in the analysis.

III. DISCUSSION

Previous workers assigned the $\nu[(h_{11/2})^2_{10}(g_{7/2})^2_6]$ configuration in ^{106}Cd [16] to band 1 above $I = 16$. Studies of the yrast positive-parity band in ^{108}Cd [17] suggest that

TABLE I. Results of the line-shape analysis for ^{106,108}Cd. τ is the mean lifetime of the state, depopulated by the γ-ray of energy E_γ. The lifetimes are the weighted average of the results obtained from the two line-shape fits from different sets of angles: ($\overline{35^\circ}$, 90°, $\overline{145^\circ}$), ($\overline{52^\circ}$, 90°, $\overline{128^\circ}$).

	$I_i \rightarrow I_f$	E_γ(keV)	τ(ps)	$B(E2)(e^2\,\mathrm{b}^2)$
^{106}Cd	$18 \rightarrow 16$	980.8	$0.60^{+0.05}_{-0.05}$	$0.15^{+0.01}_{-0.01}$
	$20 \rightarrow 18$	1150.6	$0.29^{+0.04}_{-0.04}$	$0.14^{+0.02}_{-0.02}$
	$22 \rightarrow 20$	1310.6	$0.26^{+0.02}_{-0.02}$	$0.07^{+0.01}_{-0.01}$
	$24 \rightarrow 22$	1487.6	$0.19^{+0.02}_{-0.02}$	$0.05^{+0.01}_{-0.01}$
	$26 \rightarrow 24$	1675.5	0.18[a]	0.007[a]
^{108}Cd	$12 \rightarrow 10$	556	$14.4^{+0.4}_{-0.4}$[b]	$0.11^{+0.01}_{-0.01}$
	$14 \rightarrow 12$	794	$2.2^{+0.1}_{-0.1}$[b]	$0.12^{+0.01}_{-0.01}$
	$16 \rightarrow 14$	956	$0.69^{+0.05}_{-0.04}$	$0.15^{+0.01}_{-0.01}$
	$18 \rightarrow 16$	1105	$0.33^{+0.03}_{-0.03}$	$0.14^{+0.01}_{-0.01}$
	$20 \rightarrow 18$	1260	$0.28^{+0.03}_{-0.03}$	$0.09^{+0.01}_{-0.01}$
	$22 \rightarrow 20$	1469	0.36[a]	0.03[a]

[a]The lifetime is the effective value; hence the $B(E2)$ value is the lower limit.

[b]The lifetimes of states below spin 16 in ^{108}Cd are taken from Ref. [19].

the configuration is the same above spin 16. This neutron configuration is represented by the vector $\bar{\mathbf{j}}_\nu$ in Fig. 1(b) and is coupled to the two $g_{9/2}$ proton holes, $\bar{\mathbf{j}}_{\pi^{-1}}$, whose angular momentum vectors are essentially perpendicular to the neutron angular momentum vector at $I \sim 16$.

The lifetimes deduced for states in ^{106,108}Cd have been used to calculate the $B(E2)$ transition strengths. The results are shown in Table I. In ^{106}Cd there is clear evidence of a rapid decrease in the $B(E2)$ values for the $22 \rightarrow 20$ and $24 \rightarrow 22$ transitions. Unfortunately, the data do not extend to high enough spin to be able to make the same firm conclusion for ^{108}Cd. In ^{106}Cd the positive-parity band is believed to terminate at spin 26, which is 2 units of spin beyond the termination point expected from the shears mechanism alone [9]. In this case it is assumed that the deformed core contributes 2 units of spin in the 16–26$\hbar$ range. For ^{108}Cd the band is known up to spin 24 [17]. It was not possible to observe any higher states from the present work. Furthermore, we were also unable to measure the lifetime of the spin-24 state owing to a lack of statistics for the γ ray depopulating this state. The consequence of this is that it was only possible to measure lifetimes up to spin 20. We did, however, determine the effective lifetime of the $J^\pi = 22^+$ level. The value obtained for this level (as well as the spin-26 state in ^{106}Cd) is given in Table I. These values clearly represent an upper limit for the lifetime of the uppermost states in each case and therefore result in a lower limit for the deduced $B(E2)$ values. Figure 3 shows a plot of the experimentally deduced $B(E2)$ values as a function of spin for ^{106,108}Cd. Additional data points for lower spin states in ^{108}Cd have been included using the lifetime results determined by Thorslund *et al.* [19]. Because of the symmetry of the antimagnetic configuration, the axis of rotation coincides with a principal axis. Thus, for ^{106}Cd we performed cranked Nilsson-Strutinsky (CNS) (e.g., see Ref. [20]) and tilted axis cranking (TAC) calculations [2]. In both cases the calculations were carried out without pairing. This should be a good approximation owing to the proximity of the $Z = 50$ shell gap to the proton Fermi surface and because the neutron configuration of the structure of interest involves two pairs of aligned particles, which one would expect to substantially reduce the pairing correlations. One should also note that the CNS calculations would be expected to yield similar results (see the following) to the TAC calculations since they essentially utilize the same Hamiltonian.

The prime reason for carrying out TAC calculations as well as CNS model calculations is that we were able to utilize the former to calculate the relative orientation of the $g_{9/2}$ proton hole vectors (see Simons *et al.* [9]). The results indicate that the $g_{9/2}$ proton hole spin vectors close rapidly as the spin increases from $I \sim 16$ to 26 [see Fig. 3(a)]. The deformation for the $\nu(h_{11/2})^2(g_{7/2})^2$ configuration was minimized for various rotational frequencies. At $\hbar\omega = 0.35$ ($I \sim 17$) the quadrupole deformation was found to be $\beta_2 \simeq 0.16$ and $\gamma \sim 0^\circ$, which agrees well with the results of the total Routhian surface (TRS) calculations reported in Ref. [16]. With increasing frequency the triaxiality parameter γ remained close to 0° and there was a rapid decrease of β_2, which became $\sim$0 around $\hbar\omega = 0.55$ MeV ($I \sim 26$). This is in agreement with the apparent termination of the band at spin 26, as seen in Fig. 3 of Ref. [9].

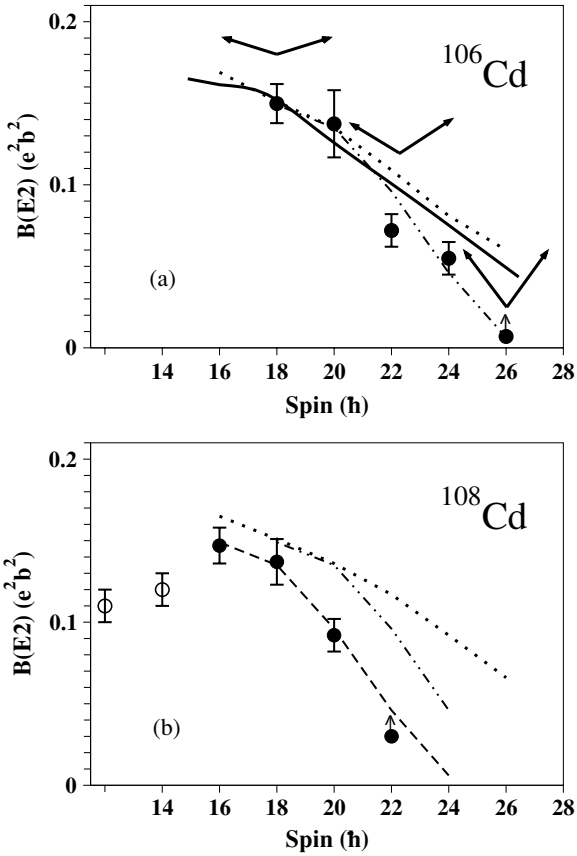

FIG. 3. Plot of $B(E2)$ values against spin for the positive-parity yrast bands in (a) ^{106}Cd and (b) ^{108}Cd. In (a) the solid line represents the $B(E2)$ values obtained from TAC calculations through minimizing the energy in the rotating frame for a range of β_2 and γ values. The arrows in this panel show the relative orientations of the $g_{9/2}$ proton hole vectors (as deduced from the TAC calculations—see text) at various spins. The dotted line in panels (a) and (b) show the results of the CNS calculations for the configuration of interest. The semiclassical model calculations shown in both panels were obtained assuming that $j_\nu = 16$ [dashed line, panel (b) only] and 18 (dot-dashed lines), respectively, as discussed in the text. Note that the data points with arrows at spin 26 [in panel (a)] and spin 22 in panel (b) represent lower limits for the $B(E2)$ values since they were calculated using the effective lifetimes of these states.

Both the CNS and TAC calculations for ^{106}Cd are in good agreement with the experimental data. Furthermore, the two calculations are also in good agreement with each other, as one might expect from models that have essentially the same Hamiltonian. The observed rapid approach to a spherical shape reflects the expectations of the shears mechanism.

Within the semiclassical model [3] description of the shears mechanism the reduced transition probability is given by

$$B(E2) = \frac{15}{32\pi}(eQ)^2_{\text{eff}} \sin^4\theta \tag{1}$$

$$= \frac{15}{32\pi}(eQ)^2_{\text{eff}} \left[1 - \left(\frac{J - j_\nu}{2j_\pi}\right)^2\right]^2, \tag{2}$$

where j_π and j_ν are the proton and neutron spin contributions, respectively, J is the total spin, and

$$(eQ)_{\rm eff} = e_\pi Q_\pi + \left(\frac{j_\pi}{j_\nu}\right)^2 e_\nu Q_\nu. \qquad (3)$$

Clark and Macchiavelli [3] deduced a value of $(eQ)_{\rm eff} = 6.5\ e\,{\rm b}$ for the magnetic-shears-type bands in the $A \sim 198$ region. In this region both protons and neutrons contribute to the value of $(eQ)_{\rm eff}$ since $j_\pi \sim j_\nu$. However, for the antimagnetic shears bands in the Cd region j_π^2 is somewhat less than j_ν^2, hence, the main contribution to $(eQ)_{\rm eff}$ comes essentially from the protons. In the present work it is found that the $B(E2)$ values are well reproduced by Eq. (2) if a value of $(eQ)_{\rm eff} = 1\ e\,{\rm b}$ is used. We have calculated the quadrupole moment for the Nilsson states using a Woods-Saxon potential at a deformation $\beta_2 = 0.17$, which is the approximate deformation deduced for ^{106,108}Cd at spin 18 and 16, respectively. These calculations yield $Q_\pi = 0.76\ e\,{\rm b}$. This suggests that we require an effective proton charge $e_\pi \sim 1.3$ to satisfy Eq. (3), which agrees reasonably well with expectations for this mass region (see, e.g., Refs. [21,22]). Figure 3(a) shows that the semiclassical model can also reproduce the experimentally observed rapid decrease of the $B(E2)$ values in ^{106}Cd. In the calculation we have taken $(eQ)_{\rm eff} = 1\ e\,{\rm b}$ and $j_\nu = 18$, which is in accordance with the experimental observation that the band appears to terminate at $J = 26$. (Note that the assumed value for j_ν is consistent with the assumption that there are 2 units of angular momentum coming from the core rotation.)

Figure 3(b) shows that the $B(E2)$ values deduced from the present work are a little higher than those obtained at lower spin (i.e., $I \leqslant 14$) from the work of Thorslund *et al.* [19]. It should be noted, however, that the measurements by Thorslund *et al.* were carried out using the recoil distance method rather than the Doppler-shift attenuation method used in the present work and that the current lifetime results are subject to stopping power uncertainties of the order of 20%, as discussed earlier. Hence it is not possible to establish with absolute certainty whether or not the observed rise in the $B(E2)$ values is a genuine effect, since there are no data points that overlap. It is, however, interesting to note that the data points shown at spin 12 and 14 in Fig. 3(b), which were both derived from the lifetime values reported by Thorslund *et al.*, suggest that there is a slight increase in the $B(E2)$ value at the higher spin. In this context we also note that in very recent work Datta *et al.* [11], who report Doppler-shift attenuation method lifetimes for states in ^{108}Cd populated via the ^{100}Mo(^{13}C,5n) reaction [11], quote a value of 1.32 (13) ps for the spin-14 state. This work utilized a lead-backed target, a feature that was also used in the present work. However, in the present work we were unable to observe any evidence for a line shape for the 794-keV γ ray that depopulates the spin-14 state. Thus from the present work the lifetime of this state would appear to be longer than that suggested in Ref. [11] and hence more in keeping with the results of Thorslund *et al.* Clearly, if the lifetime obtained by Datta *et al.* is correct it is somewhat lower than that measured by Thorslund *et al.* [19] and will of course result in an increased $B(E2)$ value ($0.19 \pm 0.02\ e^2\ {\rm b}^2$). Finally, we note that if the slight rise in the $B(E2)$ values in ^{108}Cd in the spin 12–16 region is genuine it can most likely be understood in terms of the polarizing effect of the aligning $g_{7/2}$ neutrons, which are known to align in this spin region [17,19].

The data points at spin 20 and 22 in Fig. 3(b) for ^{108}Cd tentatively suggest that the $B(E2)$ values start to fall off beyond spin 18. Unfortunately, the $B(E2)$ value given for the spin-22 state is a lower limit; hence we cannot definitively say that there is a similar drop in values to that observed in ^{106}Cd. It is clear, however, that the magnitude of the $B(E2)$ values is similar in the two nuclei before the decrease starts in ^{106}Cd.

Two sets of semiclassical model calculations are shown in Fig. 3(b) for ^{108}Cd. In one case j_ν is taken to be 18 whereas in the other $j_\nu = 16$ has been used. It is interesting to note that the calculations with $j_\nu = 16$ seem to show better agreement with the data. This is consistent with the observation that the band in ^{108}Cd is only observed up to spin 24. If all of the spin is generated by the aligning $g_{9/2}$ proton hole vectors beyond spin 16 then the maximum spin attainable is 24. The CNS calculations for ^{108}Cd, which are also shown in Fig. 3(b), reveal a similar trend to that observed for ^{106}Cd; that is, the rate at which the $B(E2)$ values decrease is less that that shown by the semiclassical model.

In well-deformed nuclei, rotation is a collective motion carried by many nucleons, each of which contributes a small fraction to the total angular momentum. The averaging over the individual nucleon contributions results in both the $\mathcal{J}^{(2)}$ and $B(E2)$ values being proportional to the square of the nuclear density distribution deformation parameter β_2. For the even more collective, superdeformed nuclei, $\mathcal{J}^{(2)}$ approaches the value expected for a rigid rotor and has a weaker deformation dependence of $\mathcal{J}^{(2)} \propto 1 + \frac{1}{2}\sqrt{\frac{5}{4\pi}}\beta_2$. In contrast, the motion of magnetic and antimagnetic rotors is carried by only a few nucleons in high-j orbitals. Their individual quantal properties are therefore not averaged out as in the case of collective rotation of well-deformed and superdeformed nuclei. This leads to a completely different relation between $B(E2)$ and $\mathcal{J}^{(2)}$, which reflects how the interaction between the high-j orbitals depends on their relative orientation. (A more quantitative comparison of magnetic and antimagnetic rotation with the familiar collective rotation can be found in Appendix A of Ref. [2].)

The experimentally observed relation between the moment of inertia $\mathcal{J}^{(2)}$ and the reduced transition probability $B(E2)$ values for the proposed antimagnetic band can be understood within both the TAC and the semiclassical description of the shears mechanism. To keep things simple, we take into account only the interaction between the $g_{9/2}$ proton holes and the $g_{7/2}$ and $h_{11/2}$ neutron particles, since the proton-neutron interaction is much stronger than the interaction between the $g_{9/2}$ proton holes. The interaction energy is assumed to be of the form

$$E(\theta) = A\cos^2\theta, \qquad (4)$$

where θ is the angle between the angular momentum vectors $\vec{\mathbf{j}}_\pi$ of the proton holes and $\vec{\mathbf{j}}_\nu$ of the neutron particles (cf.

Fig. 1). This interaction is of quadrupole type and is caused by the exchange of quadrupole phonons or, equivalently (cf. Ref. [2]), by a slight quadrupole polarization of the core, which involves all nucleons except the active high-j nucleons explicitly discussed. As demonstrated in Ref. [3], the energies of magnetic bands suggest such a quadrupole interaction. The total angular momentum is

$$J = j_\nu + 2\cos\theta j_\pi, \tag{5}$$

where $j_\nu = 16$ is the total angular momentum of the two $g_{7/2}$ and the two $h_{11/2}$ neutrons and $j_\pi = 9/2$ is the angular momentum of one $g_{9/2}$ proton hole. Hence,

$$\cos\theta = \frac{J - j_\nu}{2j_\pi} \tag{6}$$

and

$$E(J) = 2A\left[\frac{J - j_\nu}{2j_\pi}\right]^2, \tag{7}$$

where A is a constant. The rotational frequency becomes a linear function,

$$\omega(J) = \frac{A}{j_\pi^2}(J - j_\nu), \tag{8}$$

which yields a dynamic moment of inertia of

$$\mathcal{J}^{(2)} = \frac{j_\pi^2}{A}. \tag{9}$$

Thus, in the absence of any collective contributions, the latter quantity should remain constant until the band terminates at $J = 2j_\pi - 1 + j_\nu$. (Owing to the Pauli principle the two proton holes cannot completely align; see Fig. 1 in Ref. [10] for an illustration.) This prediction is in nice agreement with the experimental $\mathcal{J}^{(2)}$ values, which remain fairly constant as a function of spin and rotational frequency, This contrasts with the behavior seen in the smoothly terminating bands in ^{108}Sn and ^{109}Sb (see Fig. 4), where a definite decrease is observed as the spin (rotational frequency) increases in the region of

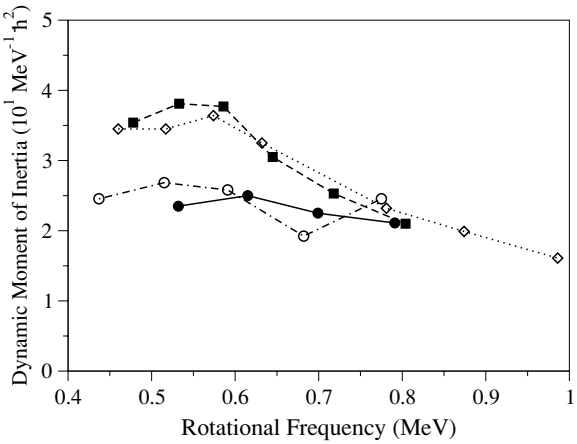

FIG. 4. Plot of the dynamic moment of inertia $\mathcal{J}^{(2)}$ vs spin for the antimagnetic bands in ^{106}Cd (filled circles), ^{108}Cd (open circles), and two of the smoothly terminating bands in ^{108}Sn (filled squares) and ^{109}Sb (open diamonds).

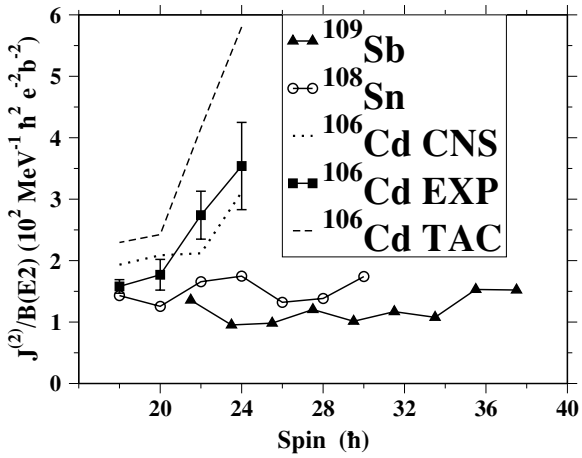

FIG. 5. Plot of the $\mathcal{J}^{(2)}/B(E2)$ ratio vs spin for the antimagnetic band in ^{106}Cd and two of the smoothly terminating bands in ^{108}Sn and ^{109}Sb (using data taken from Ref. [23]). Also shown are the values obtained from the TAC and CNS calculations.

interest. Furthermore, since the $B(E2)$ values are expected to decrease rapidly with increasing spin the $\mathcal{J}^{(2)}/B(E2)$ ratio should show a rapid increase. The experimental $\mathcal{J}^{(2)}/B(E2)$ ratio is shown in Fig. 5 for ^{106}Cd along with the predictions from the CNS and TAC models and the experimental values for some of the smoothly terminating bands in ^{109}Sb and ^{108}Sn. Data for the latter are taken from Ref. [23]. The steep rise observed in the experimental values is characteristic for antimagnetic rotation, reflecting the fact that $\mathcal{J}^{(2)}$ is essentially constant whereas the $B(E2)$ values rapidly approach zero as the spin increases along the band. The experimental data for the two smoothly terminating bands in ^{108}Sn and ^{109}Sb have an almost constant $\mathcal{J}^{(2)}/B(E2)$ ratio, indicating that the two quantities have a similar behavior with deformation as the spin increases. Given the well-known difficulties in calculating $\mathcal{J}^{(2)}$ values the calculations show quite good agreement with the experimentally deduced values.

IV. CONCLUSIONS

The lifetimes of states in the lowest lying positive parity bands in ^{106,108}Cd have been studied by means of the Doppler-shift attenuation method technique. The $B(E2)$ values derived for ^{106}Cd show a rapid decrease with increasing spin and a remarkable agreement with the CNS, TAC, and semiclassical model calculations. TAC calculations for ^{106}Cd predict that following the initial alignment of the $h_{11/2}$, $g_{7/2}$ neutrons at spin 16 the $g_{9/2}$ proton hole vectors are almost antiparallel. As the spin increases these vectors gradually close on the aligned neutron vectors and the spherical symmetry is restored. In ^{108}Cd the situation is a little less clear since in this case there is only one data point showing evidence for a decrease in the $B(E2)$ values beyond spin 20. Nevertheless, the suggestion remains that the antimagnetic shears mechanism is active in this case also. Finally, the present work has demonstrated that in antimagnetic rotors $\mathcal{J}^{(2)}$ is nearly constant whereas

$B(E2)$ values decrease with increasing angular momentum. This behavior, which contrasts that of normal rotors, where the $\mathcal{J}^{(2)}$ and $B(E2)$ values are approximately proportional to each other, has been explained as a consequence of the shears mechanisms being the main source of angular momentum generation.

ACKNOWLEDGMENTS

We thank the staff of the 88-In. Cyclotron and R. Darlington for the production of the targets. This work was supported in part by the U.S. DOE under Contract No. DE-AC03-76SF00098, the UK EPSRC.

[1] A. Bohr, Mat. Fys. Medd. K Dan. Vidensk Selsk. **26**, 1 (1952).
[2] S. Frauendorf, Rev. Mod. Phys. **73**, 463 (2001).
[3] R. M. Clark and A. O. Macchiavelli, Annu. Rev. Nucl. Part. Sci. **50**, 1 (2000).
[4] R. M. Clark *et al*., Phys. Rev. Lett. **82**, 3220 (1999).
[5] D. G. Jenkins *et al*., Phys. Rev. Lett. **83**, 500 (1999).
[6] S. Chmel, F. Brandolini, R. V. Ribas, G. Baldsiefen, A. Gorgen, M. De Poli, P. Pavan, and H. Hubel, Phys. Rev. Lett. **79**, 2002 (1997).
[7] S. Frauendorf, Nucl. Phys. **A557**, 259c (1993).
[8] S. Frauendorf, in *Proceedings of the Workshop on Gammasphere Physics, Berkeley*, edited by M. A. Deleplanque, I. Y. Lee, and A. O. Macchiavelli (World Scientific, Singapore, 1995), p. 272.
[9] A. J. Simons *et al*., Phys. Rev. Lett. **91**, 162501 (2003).
[10] S. Zhu *et al*., Phys. Rev. C **64**, 041302(R) (2001).
[11] P. Datta *et al*., Phys. Rev. C **71**, 041305(R) (2005).
[12] I. Y. Lee, Nucl. Phys. **A520**, 641c (1990).
[13] J. C. Wells and N. Johnson (private communication), (1998).
[14] J. Gascon *et al*., Nucl. Phys. **A513**, 344 (1990).
[15] L. C. Northcliffe and R. F. Schilling, Nucl. Data Tables **7**, 233 (1970).
[16] P. H. Regan *et al*., Nucl. Phys. **A586**, 351 (1995).
[17] I. Thorslund *et al*., Nucl. Phys. **A564**, 285 (1993).
[18] F. James *et al*., Comput. Phys. Commun. **10**, 343 (1975).
[19] I. Thorslund *et al*., Nucl. Phys. **A568**, 306 (1994).
[20] A. V. Afanasjev, D. B. Fossan, G. J. Lane, and I. Ragnarsson, Phys. Rep. **322**, 1 (1999).
[21] D. Alber *et al*., Z. Phys. A **335**, 265 (1990).
[22] L. Coraggio, A. Covello, A. Gargano, N. Itaco, and T. T. S. Kuo, J. Phys. G **26**, 1697 (2000).
[23] R. Wadsworth *et al*., Phys. Rev. Lett. **80**, 1174 (1998).